

# Spatio-temporal dynamics of cerebral capillary segments with stalling red blood cells

Şefik Evren Erdener<sup>1</sup>, Jianbo Tang<sup>1</sup>, Amir Sajjadi<sup>1</sup>, Kivılcım Kılıç<sup>2</sup>, Sreekanth Kura<sup>1</sup>, Chris B Schaffer<sup>3</sup> and David A Boas<sup>1,2</sup>

## Abstract

Optical coherence tomography (OCT) allows label-free imaging of red blood cell (RBC) flux within capillaries with high spatio-temporal resolution. In this study, we utilized time-series OCT-angiography to demonstrate interruptions in capillary RBC flux in mouse brain in vivo. We noticed ~7.5% of ~200 capillaries had at least one stall in awake mice with chronic windows during a 9-min recording. At any instant, ~0.45% of capillaries were stalled. Average stall duration was ~15 s but could last over 1 min. Stalls were more frequent and longer lasting in acute window preparations. Further, isoflurane anesthesia in chronic preparations caused an increase in the number of stalls. In repeated imaging, the same segments had a tendency to stall again over a period of one month. In awake animals, functional stimulation decreased the observance of stalling events. Stalling segments were located distally, away from the first couple of arteriolar-side capillary branches and their average RBC and plasma velocities were lower than nonstalling capillaries within the same region. This first systematic analysis of capillary RBC stalls in the brain, enabled by rapid and continuous volumetric imaging of capillaries with OCT-angiography, will lead to future investigations of the potential role of stalling events in cerebral pathologies.

## Keywords

Microcirculation, capillary, blood flow, stall, optical coherence tomography

Received 28 July 2017; Revised 9 October 2017; Accepted 30 October 2017

## Introduction

The high metabolic demand of the cerebral cortex requires a continuous oxygen supply through the vascular network. The dense capillary mesh within the cerebral microcirculation permits efficient oxygen delivery as the typical distance between neurons and capillaries is 8–20  $\mu\text{m}$ .<sup>1</sup> Diseases affecting small vessels in the brain cause a decrease in cerebral blood flow with a reduced oxygen availability in the brain.<sup>2–4</sup> It is necessary but challenging to image the microcirculation in high spatio-temporal resolution due to the size and complexity of capillaries. Indeed, advanced capillary imaging has proven to be very useful for increasing our understanding of the microcirculation in health<sup>5–9</sup> and disease.<sup>10–16</sup> An interesting mechanism of microcirculatory dysfunction was identified by two-photon microscopy (TPM) in mouse models of myeloproliferative disease, where spontaneous stalls in capillary red blood cell (RBC) flux in individual capillary segments

were observed.<sup>17</sup> Similar stall events were also previously seen in cerebral and retinal capillaries<sup>18–20</sup> but were not systematically analyzed. Excessive amounts of these flow interruptions would decrease oxygen availability and would potentially result in neuronal injury.

<sup>1</sup>Optics Division, Athinoula A. Martinos Center for Biomedical Imaging, Massachusetts General Hospital, Harvard Medical School, Charlestown, MA, USA

<sup>2</sup>Neurophotonics Center, Department of Biomedical Engineering, Boston University, Boston, MA, USA

<sup>3</sup>Meinig School of Biomedical Engineering, Cornell University, Ithaca, NY, USA

## Corresponding author:

Şefik Evren Erdener, Optics Division, Athinoula A Martinos Center for Biomedical Imaging, Department of Radiology, Massachusetts General Hospital, Harvard Medical School, 149 13th Street, Charlestown, MA 02129, USA.

Email: evrenerdener@gmail.com

Although TPM can demonstrate RBC stalls,<sup>17</sup> the relatively narrow field of view, the requirement for repeat planar imaging to visualize a volume, and the slow acquisition speed make it difficult to gather simultaneous data from multiple capillary segments. Further, it requires an excessive amount of data and effort to quantify these stalling events on a wide scale. TPM also requires injection of contrast agents and besides animal stress, this can possibly influence blood viscosity or the vessel walls. Optical coherence tomography (OCT) allows continuously repeated volumetric angiographic imaging at a high-speed and with capillary-level resolution without the need for exogenous contrast.<sup>21,22</sup> In this study, we utilized OCT-angiogram time-series to detect and quantify capillary stalls for an extended period of time (up to 18 min) and with high temporal resolution ( $\sim 0.1$  Hz), permitting the continuous imaging of  $\sim 200$  capillaries. We describe and compare these stall parameters in both anesthetized and awake mice, with both acute and chronic window preparations, to test the applicability of our technique in various models. OCT permits efficient characterization of the spatio-temporal dynamics of these stall events. For a cerebral physiological perspective, we show that the stalls are modulated during functional activation. We anticipate that in future studies, this method will permit association of these stalling events with various small vessel and neurodegenerative diseases.

## Methods

### *Animals and surgery*

For acute imaging, two to three-month-old CD1 mice (23–26 g, female, Charles River) were used. Animals were housed under diurnal lighting conditions with free access to food and water. Under isoflurane anesthesia (2–3% induction, 1–2% maintenance, in 25/75% oxygen/air), the left femoral artery was cannulated for blood pressure measurements. Body temperature was maintained with a homeothermic unit (Harvard Apparatus). A craniotomy ( $3 \times 3$  mm) was performed over the left somatosensory cortex and the dura was removed. The cortex was covered with agarose (1% in saline), then with a 5-mm diameter glass. The window was sealed with dental cement. The animal was then placed under the imaging system.

For chronic awake imaging, C57BL/6 mice (20–23 g, female, Charles River) underwent surgery when they were 12-weeks old. A  $3 \times 3$  mm craniotomy was performed over the left somatosensory cortex, keeping the dura intact. A glass plug was inserted into the craniotomy and fixed with dental acrylic (see supplementary methods for details). Mice recovered for two weeks

after surgery, followed by an additional two weeks for the training of the mice to tolerate head restraint. The first imaging sessions were performed when mice were  $\sim 4$  months old (at least one month after surgery).

All experiments were approved by the Massachusetts General Hospital Subcommittee on Research Animal Care, were conducted following the Guide for the Care and Use of Laboratory Animals and reported in compliance with the ARRIVE guidelines.

### *OCT system and imaging protocol*

A spectral-domain OCT system (1310 nm center wavelength, bandwidth 170 nm, Thorlabs) was used for imaging of the cerebral cortex.<sup>22</sup> Axial resolution of the system was  $3.5 \mu\text{m}$  and imaging speed was 47,000 A-scan/s. A  $10\times$  objective was used allowing a transverse resolution of  $3.5 \mu\text{m}$ .

OCT-angiograms were constructed by a decorrelation-based method.<sup>22</sup> While conventional structural OCT imaging acquires one  $xz$  B-scan for each  $y$  position, the decorrelation-based method repeats two B-scans and then analyzes the differences in the image intensity and phase between the repeated B-scans. There will be no difference for repeated voxels for static tissue. In contrast, dynamic tissue, such as a blood vessel, will experience a large intensity/phase difference between repeated B-scans due to particle movement (e.g. flowing RBCs), and will appear as bright areas in the OCT-angiogram.

For each experiment, two regions of interest (ROI) ( $600 \times 600 \mu\text{m}^2$ ) were imaged during baseline conditions. The ROI was raster scanned at  $400 \times 400$  pixel resolution. Each OCT-angiogram acquisition took  $\sim 9$  s, and a time-series of 60 volumes of the cortical microvasculature was consecutively acquired for each ROI. In a subgroup of experiments, we repeated B-scans five times to assess the detection sensitivity to slow moving RBCs by using different B-scan intervals.

Maximum intensity projections (MIPs) of each angiogram  $150$ – $250 \mu\text{m}$  beneath the brain surface were extracted for analysis as these layers provided a high-quality angiogram signal from capillaries. In angiograms, stalling capillary segments were readily identified as a sudden intensity drop; disappearance and reappearance of flowing RBCs in individual segments could be observed. We marked and manually counted each stall for quantification.

For repeated experiments, we imaged the capillaries in the same ROIs at the same depth. In paired awake/anesthetized experiments, oxygen/air was supplied to the animal during the awake recording, then isoflurane was added at the aforementioned dose; imaging was done  $\sim 5$  min after establishment of anesthesia with maintenance of body temperature.

### Statistical analyses

Stall incidence was calculated by the number of segments stalling any time in the time-series divided by the total number capillaries. Stall point prevalence indicated the average number of stalled segments in each imaging frame divided by the total number of capillaries. Cumulative stall duration was expressed as the percentage of time that a given stalling capillary segment was not flowing. Independent groups were compared by Kruskal–Wallis ANOVA, followed by Kolmogorov–Smirnov test or by Mann–Whitney (independent samples). Dependent comparisons were done by Friedman test followed by Wilcoxon tests (dependent samples). Branching order distributions were compared by Chi-square test.  $P < 0.05$  was accepted

as statistically significant. Results were expressed as mean  $\pm$  standard deviation, unless otherwise indicated.

## Results

### Identification of stalls

Repeated imaging with time-series OCT-angiography allows the detection of flowing capillaries at a given time point and permits comparison across the images to identify transiently stalling segments. In all monitored ROIs, we identified a considerable number of stall events in a fraction of capillary segments (Figure 1). Stalls occurred preferably in certain segments, some of which stalled more frequently than

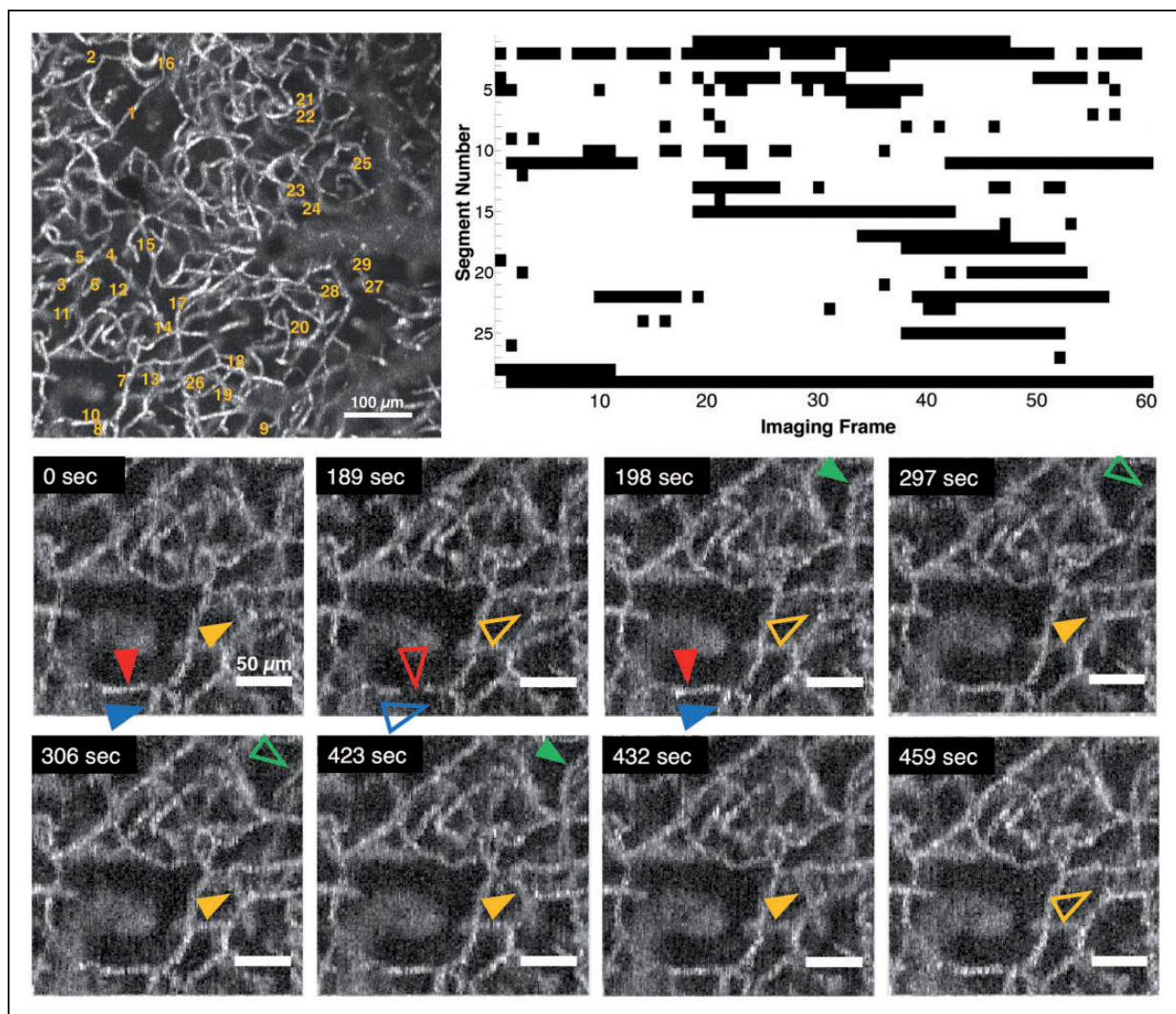


**Figure 1.** Representative OCT angiogram of capillary segments with stalling RBCs. Top left: Full field angiogram with stalling segments indicated with numbers. Scalebar: 100  $\mu\text{m}$ . Top right: Timeline of stalling segments through 60 consecutive images ( $\sim 9$  min). Black points denote stalls. Bottom: Individual segments (arrowheads) with temporary interruptions of RBC flux (zoom in of the ROI in the top-left image). Hollow arrowheads indicate a stalled capillary segment. Scalebar: 50  $\mu\text{m}$ .

**Table 1.** Stall parameters across experimental groups.

	Acute cranial window ( <i>n</i> = 6)	Chronic cranial window and awake animals (~4-month-old, <i>n</i> = 7)	Chronic cranial window and awake animals, before anesthesia (~7-month-old, <i>n</i> = 6)	Chronic cranial window and 5 min after anesthesia ( <i>n</i> = 6)
Stall incidence (in 9 min of observation) Acute-chronic <i>p</i> = 0.002 Awake-anesthetized <i>p</i> = 0.007	18.6 ± 8.7% of all capillaries	7.50 ± 2.56% of all capillaries	6.8 ± 2.9% of all capillaries	11.9 ± 3.1% of all capillaries
Number of stalls in each segment (in 1 min) Acute-chronic <i>p</i> = 0.01 Awake-anesthetized <i>p</i> = 0.14	0.55 ± 0.39	0.25 ± 0.06	0.31 ± 0.07	0.28 ± 0.08
Stall duration Acute-chronic <i>p</i> = 0.001 Awake-anesthetized <i>p</i> = 0.54	49.3 ± 21.1 s	15 ± 4.5 s	23 ± 15 s	29 ± 18 s
Point prevalence (at each time point) Acute-chronic <i>p</i> = 0.002 Awake-anesthetized <i>p</i> = 0.01	3.4 ± 1.5% of all capillaries	0.45 ± 0.35% of all capillaries	0.6 ± 0.2% of all capillaries	1.5 ± 0.6% of all capillaries
Cumulative stall duration Acute-chronic <i>p</i> = 0.002 Awake-anesthetized <i>p</i> = 0.54	19.8 ± 6.0% of observed time	5.8 ± 1.9% of observed time	10.6 ± 3.2% of observed time	11.9 ± 6.2% of observed time

others. We called these “stalling segments.” A different subset of capillaries was stalled at each time point. The stalling segments did not have any distinguishing feature that could be readily identified from the OCT images.

In experiments with anesthetized acute cranial window preparations (*n* = 6), the stall incidence, i.e. percentage of capillaries having a stall any time during the 9-min recording, was around 19% (see Table 1 for statistics). Stalls were occurring on average once every 2 min for a given stalling segment, and the interruption of flow lasted for ~50 s. At each imaging time point, 3.4% of the visible capillary segments were stalled (point prevalence of stalls). As acute cranial surgery and anesthesia would have an impact, we performed experiments using awake mice with chronic cranial windows, at rest (*n* = 7). In these animals, capillary stall events were less frequent, but still consistently being observed. In awake mice, the stall incidence was 7.5%, occurring on average once every 4 min for each stalling segment with a duration of ~15 s on average (Table 1). For each imaging time point, 0.45% of the capillary segments were observed to be stalled. Differences in these stall parameters between acute and chronic animal groups were significant. These statistics were acquired from all upstream and downstream capillary segments visible in the ROI.

### Temporal dynamics of capillary stalls

We compared the distributions of all stalling segments in terms of stall frequency (observed stalls in 9 min) and cumulative stall duration for both the acute (*n* = 348 segments) and the chronic/awake (*n* = 252 segments) studies. Figure 2(a) and (b) shows the probability distribution function of the stall frequency and cumulative stall duration. The distributions for acute and chronic/awake mice were different, with acute mice having a larger stall frequency and cumulative stall duration. Less than 2% of these segments in the awake group were cumulatively stalling for over 300 s, while more than 10% of the segments cumulatively stalled for over 300 s in the acute/anesthetized group. Aggregating the acquired image ROIs from the chronic awake animals (14 ROIs), we found no correlation between stall incidence and average cumulative stall duration ( $R^2 = 0.1482$ , *p* = 0.174, Figure 2(c)), suggesting that a higher number of involved capillaries did not necessarily mean that these capillaries would be stalling for longer durations.

Since we observed a difference in stall parameters between acute/anesthetized mice and chronic/awake mice, we tested another group of animals to evaluate the effect of isoflurane anesthesia alone. We compared stall events immediately before and 5 min

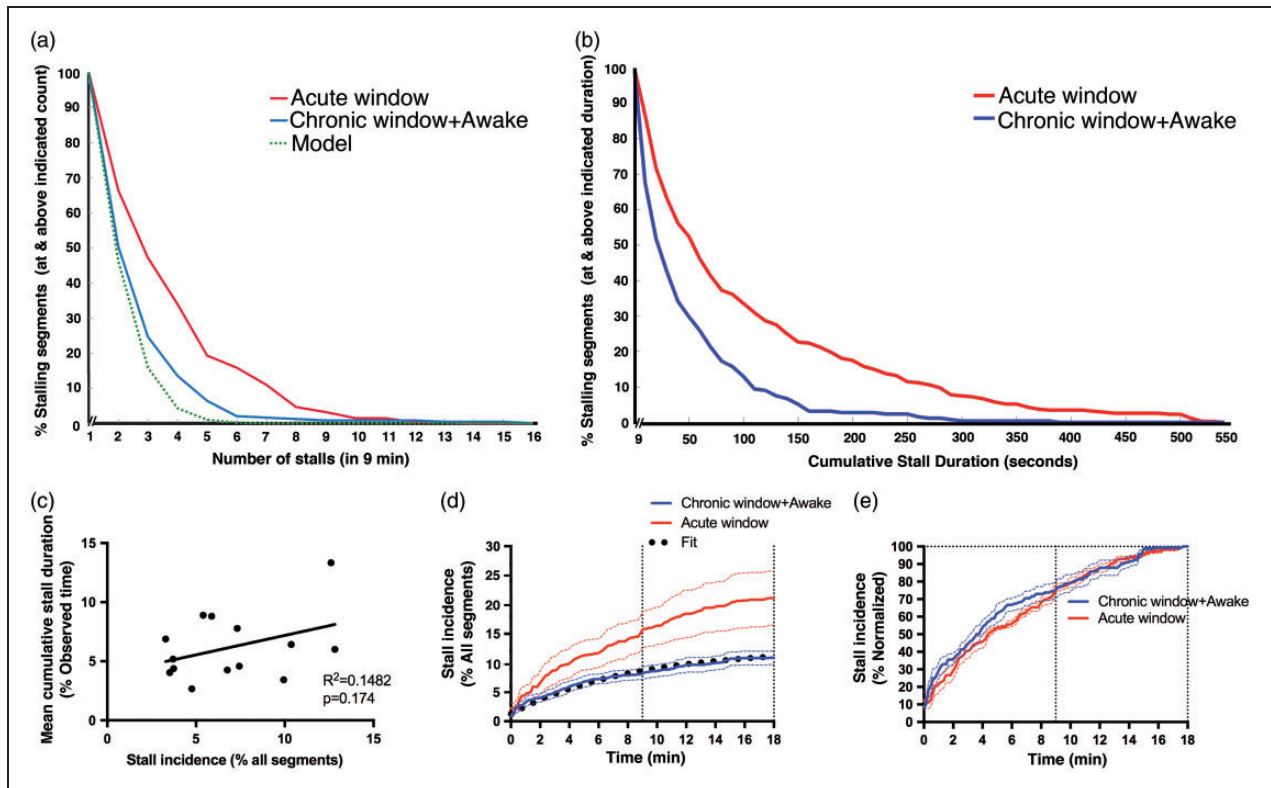


**Figure 2.** Temporal dynamics of capillary stalls. (a–b) Distribution of stall counts and cumulative stall durations of each segment in acute (anesthetized) and chronic (awake) cranial windows during a 9-min observation. Model prediction is seen as a green dotted curve in (a). (c) Lack of correlation of stall incidence with average cumulative stall duration (per ROI) for awake animal recordings. (d–e) Identified percentage of stalls relative to all observed segments (d) or all identified stalling segments (e) as a function of observation time (imaging time extended to 18 min). Exponential fit is seen as black dotted curve in (d).

after establishment of anesthesia in mice with chronic surgery ( $n=6$ , one prior animal was excluded due to poor cranial window quality). These experiments were done  $\sim 3$  months after the initial set of experiments, which may account for the slightly different baseline characteristics. We observed that isoflurane significantly increased the stall incidence (11.9% vs. 6.8%) and point prevalence of stalls (1.5% vs. 0.6%) compared to the awake state, but that stall frequencies and durations were not different (Table 1).

When we plotted the cumulative stall incidence versus image acquisition time, we noticed that the total number of stalling segments was still increasing after 9 min (Figure 2(d) and (e)). We thus extended the measurement duration to 18 min in both chronic/awake ( $n=6$ ) and acute/anesthetized animals ( $n=4$ ). Cumulative stall incidence over the 18-min observation time revealed that the first 9 min identified about 75% of all observed stalling segments, and that the number of stalling segments was likely still increasing after 18 min (Figure 2(d) and (e)).

### Repeatability of observed capillary stalls

Next, we aimed to quantify the degree to which capillaries would repeatedly stall. We started by comparing the stalls within the same ROI between two immediately repeated 9-min time-series in awake mice ( $n=6$ ), the second one initiated about 1 min after the first one was completed. Only 65% of stalling capillaries were common in both recordings, although the total stall incidence was similar (7.3% vs. 7.0%) in both cases. This could be explained simply by the previous observation that not all capillaries stall within a given 9-min interval. We then explored if this repeatability of stalling segments would be maintained over days and weeks. In awake animals, we repeated measurements within the same ROI, with one-day, one-week and one-month intervals, to see what fraction of stalling segments was common in the repeated sessions (Figure 3(a) and (c)). We found that  $\sim 50\%$  of previously stalling capillaries were exhibiting stalls again. For these repeated measurements, there was no significant difference in the stall incidence, and there was no

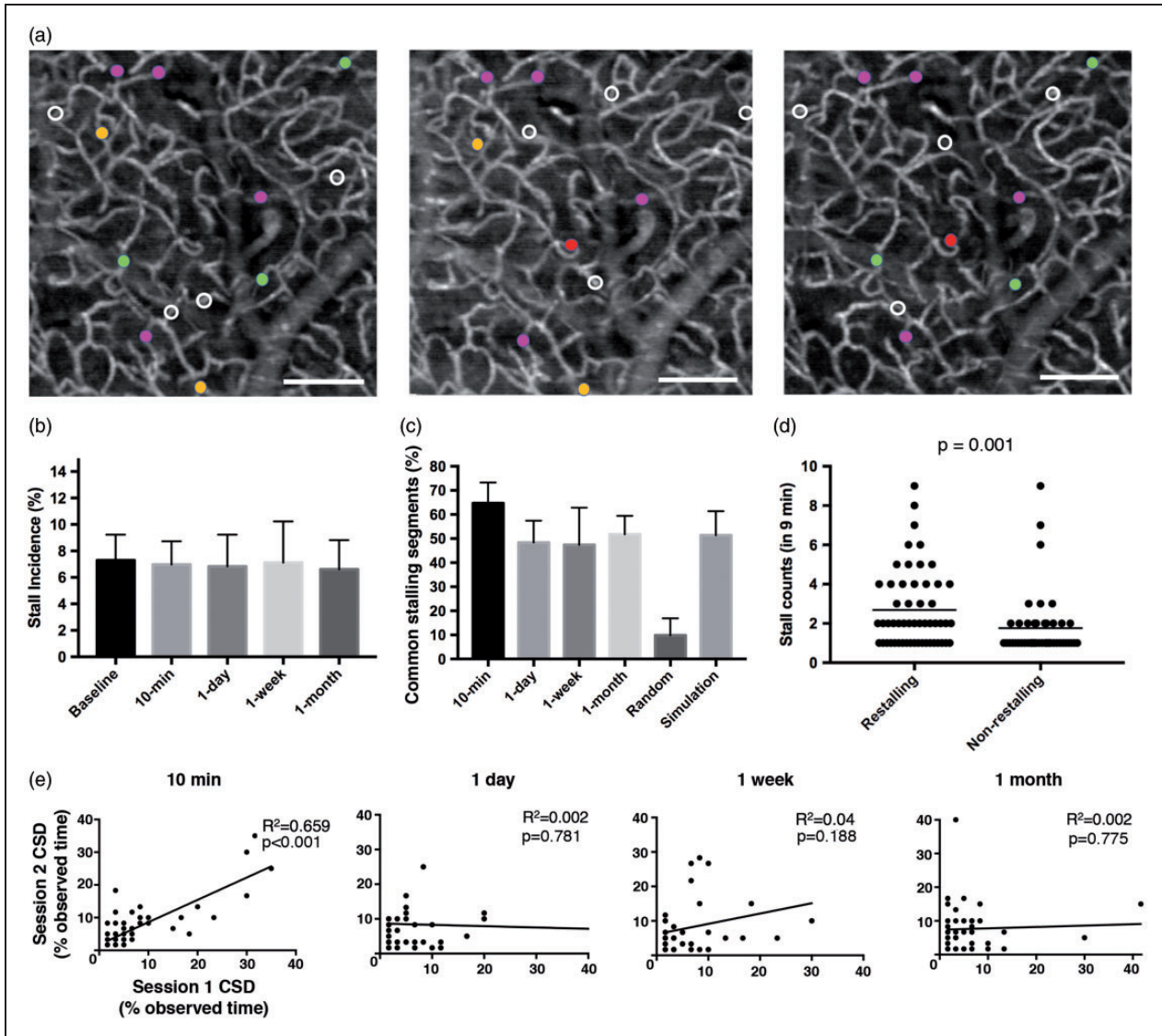


**Figure 3.** Repeatability of capillary stalls (a) representative angiogram at baseline, at one week and at one month later showing segments that were observed to stall during each session. Stalling segments that are common across different imaging sessions are marked with the same color circle. White circles indicate segments that were only observed to stall in that given imaging session. Scalebar: 100  $\mu$ m. (B) Comparison of stall incidence in awake mice across different imaging sessions. (c) Percentage of common stalling segments across different imaging sessions defined as the number of common stalling segments divided by the mean number of stalling segments in the two imaging sessions. No significant difference was observed between imaging sessions, but 10-min recording intervals had a higher percentage of overlapping segments. Common stall percentages were high compared to a random model of stall overlap percentage. Prediction of overlapping segment percentage by our model of stall kinetics matched the actual measured common stalling segment ratio, indicating that the same capillaries stall in repeated imaging sessions. (d) Re-stalling segments have a significantly higher stall frequency compared to non-re-stalling segments. (e) Cross-correlations of stall counts for the overlapping segments between repeated recordings at 10 min, one-day, one-week and one-month intervals. We observed a weak but significant correlation in the overlapping segments for the 10 min repeated recording but there was no correlation for the longer intervals, which may explain the relatively higher percentage of common stalling segments observed in 10-min repeats.

apparent change in the morphology of the capillary network over time (Figure 3(a)). The segments with a higher stall frequency in the first session had a significantly higher probability of being detected as a stalling capillary in the repeated session (Figure 3(d)).

Comparing restalling and nonrestalling segments, we did not find significant difference in segment length ( $89 \pm 5 \mu$ m vs.  $92 \pm 16 \mu$ m, respectively) or tortuosity indices<sup>23</sup> ( $1.45 \pm 0.1$  vs.  $1.41 \pm 0.1$ , respectively). We also did not visually identify a distinguishing

phenotype. This implies that the propensity of certain segments to stall repeatedly is not a result of their geometry.

We calculated what percent of capillaries would be commonly stalled in two repeated occasions, if they were selected randomly from the same pool of  $\sim 200$  capillary segments. We applied the measured percentage of stalling capillaries and randomly assigned capillaries in two different imaging sessions accordingly. We found that only  $\sim 10\%$  of stalled capillaries would be common between imaging sessions by chance alone. In fact, a significantly higher number of stalling capillaries were overlapping between imaging sessions ( $p < 0.001$ ), suggesting that certain capillary segments were more prone to stalls than others.

### Modeling the temporal dynamics of stalls

We developed a simple model to help us understand if the 50% overlap of stalled capillary segments after one day, one week and one month was expected given the cumulative stall incidence versus time in Figure 2(c), or if we would expect a higher percent overlap. If our model predicts the 50% overlap, then it suggests that the specific capillary segments that stall do not change over the one day and longer intervals. It would suggest that if we were to measure all of the stalled capillaries, which would require perhaps a 1 or 2-h experiment, then we would observe 100% overlap. If instead, our simple model predicts a higher percent overlap, then it indicates that different capillaries are stalling after one day and longer. We might expect that different capillaries are stalling after one day and longer because the 10-min interval has a 65% overlap. We fit the chronic window cumulative stall incidence data in Figure 2(c) with a simple exponential model

$$I_{stall} = A(1 - \exp(-t/B)) + C \quad (1)$$

where  $A + C$  is the total stall incidence,  $C$  is the point prevalence of stalls at any given time point,  $B$  is the time constant for a stall to happen in any given capillary that experiences stalls, and  $t$  is the experiment time. The best fit gave us  $A = 11\%$ ,  $B = 8$  min, and  $C = 1.25\%$  (see the dotted line fit in Figure 2(c)), indicating that a total of 12.25% of the capillaries would stall if we measured long enough to observe all of the stalling capillaries.

We then performed a Monte Carlo simulation calculating when a given stalling capillary would have its stalling events where initially  $C$  percent of the capillaries were stalled, and the time intervals for subsequent stall events for each capillary were drawn from a random sample of an exponential probability distribution function given by the time constant  $B$ .

The cumulative stall incidence predicted by the simulation matches equation (2), as expected. We could then calculate different random instances of which of the  $A + C$  capillaries would stall in a given 9-min experiment and calculate the percent overlap of capillaries that stall in two different instances. The model predicts an overlap of  $51\% \pm 10\%$ , which matches well with our observed overlap of  $51.7 \pm 7.7\%$ . This implies that the same capillaries are stalling even after one month from the original measurement and that we only measure a 50% overlap simply because the recording session was not long enough. The model predicts that if we measured for 18 min instead of 9 min, that we would measure an 82% overlap.

We need to explain the larger 65% overlap when the 9-min measurement was immediately repeated. We suspected that capillaries that stalled had a higher propensity to stall again over this short time span of 20 min. We calculated the cross-correlation of cumulative stall durations of common stalling segments in the 1st and 2nd sessions for varying interval recordings. There was a significant correlation between consecutive recordings for 10-min repeats (Figure 3(e)) but no correlation for longer intervals (one day, one week, one month), confirming our hypothesis that the stall kinetics of given capillaries were similar within 10 min after the initial recording but not after longer intervals. To further confirm this, we used our model to predict the plot in Figure 2(a) which shows the percent of stalling capillaries with a frequency greater than  $X$  stalls per 9 min recording. The prediction is shown by the dotted line in Figure 2(a) and indeed the model underestimates the experimentally observed stalling frequency distribution, confirming our expectation that capillaries that experience a stall are more likely to stall again on this short time frame.

### Effect of functional stimulation on stalls

We performed whisker stimulation experiments ( $n = 6$ ) simultaneously with OCT angiogram time series acquired over the barrel cortex in awake animals in order to assess whether capillary stalls would be affected by increased blood flow during functional activation, which was confirmed with laser speckle contrast imaging (Figure 4(a)) (see supplementary methods). We then compared stall incidences and point prevalences of stalls in the 5-frame-epochs before, during and after stimulation. Although stalls could still be observed during sensory stimulation, their average incidence, prevalence and cumulative durations were significantly lower during the stimulus than during the pre-stimulus period (incidence:  $1.27 \pm 0.68\%$  vs.  $0.64 \pm 0.3\%$  of all segments,  $p = 0.018$ ; prevalence:  $0.47 \pm 0.23\%$  vs.  $0.2 \pm 0.09\%$  of all segments,  $p = 0.012$ ; cumulative

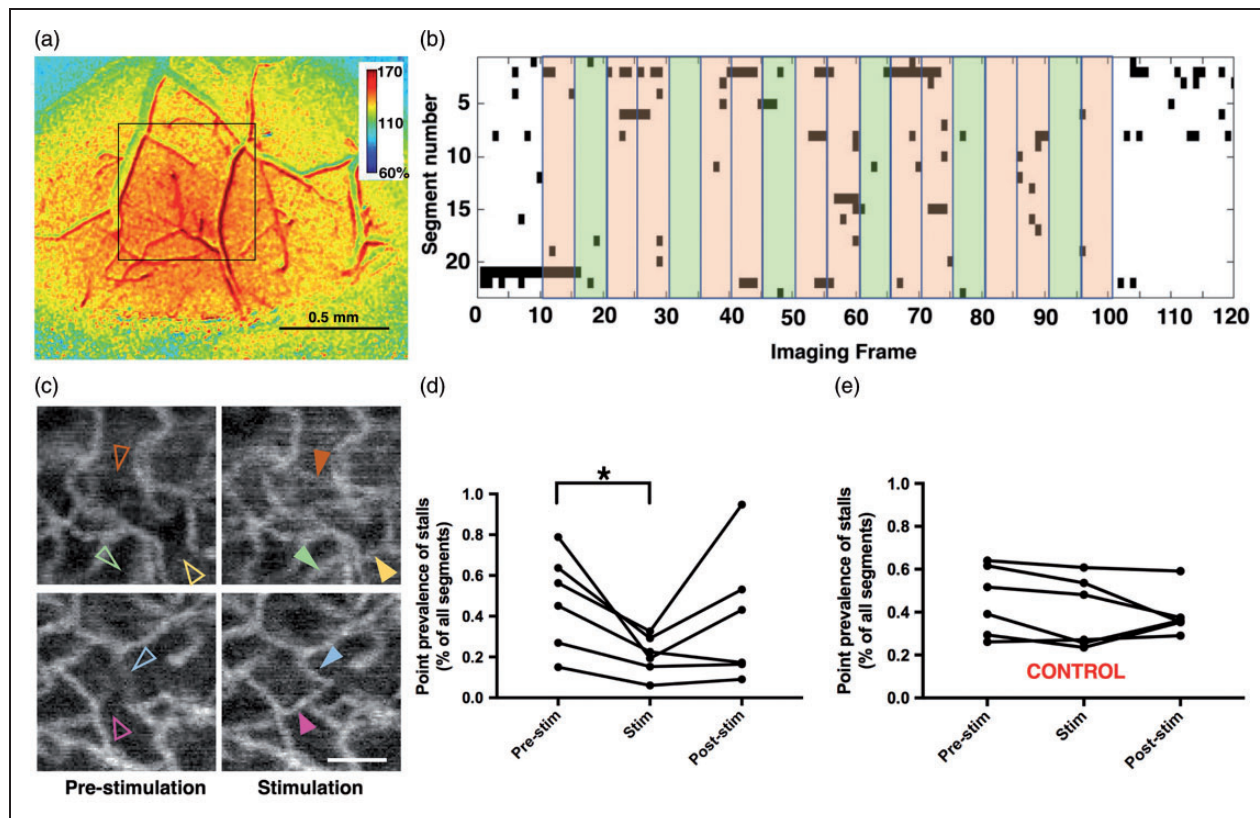


**Figure 4.** Functional modulation of capillary stalls. (a) Laser speckle contrast imaging over the OCT region of interest (black square), confirming the functional hyperemia in the relative blood flow images. (b) Matrix plot of individual stall events during the course of OCT angiogram time series, acquired from a single experiment. Black points denote the stalls. Each row represents a different segment of interest. Green shades mark the epochs during whisker stimulation, while pink shades show the pre-stimulation periods or post-stimulation epochs. (c) In selected ROIs, angiograms averaged over five frames during pre-stimulation and stimulation periods revealed segments (arrowheads) appearing during whisker stimulation that had a stall in the pre-stimulation phase. Scalebar: 50  $\mu\text{m}$ . (d) Case-by-case plots of average point prevalence of stalls during pre-stimulation, stimulation and post-stimulation epochs. Stall prevalence was significantly lower during the stimulation period compared to pre-stimulation. (e) There was no significant difference between the acquisition frames corresponding to these epochs in the control group, in which no external whisker stimulation was applied.

duration:  $6.6 \pm 2.6\%$  vs.  $3.6 \pm 1.6\%$  of epoch,  $p = 0.017$ ; for pre-stimulus and stimulus, respectively) (Figure 4(d)). The incidence ( $1.01 \pm 0.69\%$ ), prevalence ( $0.38 \pm 0.32\%$ ) and cumulative duration ( $5.4 \pm 2.8\%$ ) in the post-stimulus period was also relatively higher than the stimulus, but it did not reach statistical significance in post hoc analyses. In the control group ( $n = 6$ ), virtually no difference in any parameter between the corresponding OCT epochs was observed ( $p > 0.05$ ) (Figure 4(e)).

#### Location of stalls within the microcirculatory network

We next quantified the spatial differences between stalling and nonstalling capillary segments. In awake animals ( $n = 5$ ), we acquired two-photon-microscopy angiograms spatially overlapping with the OCT-angiograms (see supplementary methods). TPM angiograms have a higher spatial resolution and signal-to-noise

ratio and better enabled us to determine the branch orders of the segments relative to the feeding arterioles and draining venules within the microcirculatory network (Figure 5). In our imaging areas, capillary branching orders ranged from A1 to A5 (after the penetrating arteriole) and V1 to V5 (before the ascending venule). We did not count more than five branch orders from arterioles/venules as we were not confident that such segments were not closer to arterioles or venules outside of our field of view given that on average there are eight capillary branches between the penetrating arterioles and veins in mice.<sup>24–26</sup> Therefore, our sampling of segments here does not involve comprehensive tracing of the whole vascular network where high branch-order capillaries would be actually more numerous than indicated. Each capillary segment was counted only once as being closer to an arteriole or venule. The stalling segment distribution largely tracked the distribution of capillaries, but with a bias away from the first

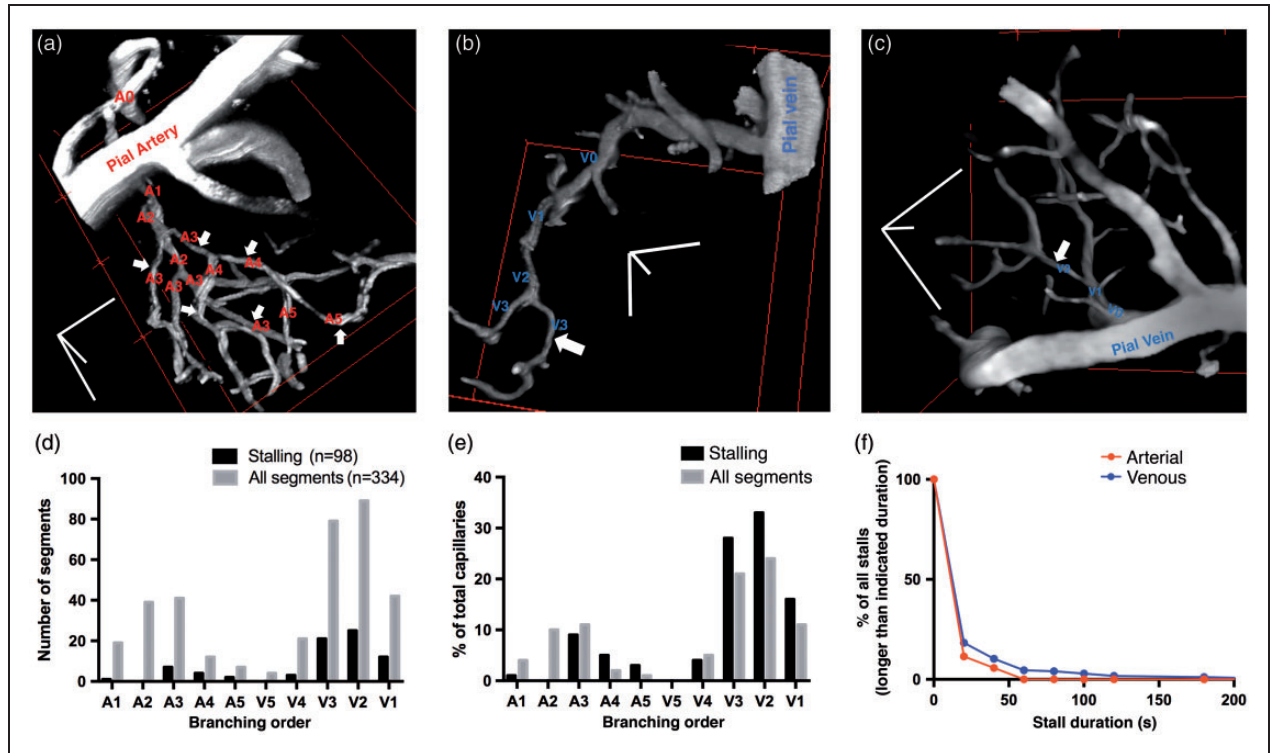


**Figure 5.** Stall locations within the microcirculatory network. (a–c) Example 3D TPM reconstructions of capillaries showing their position and sequential branch orders relative to a penetrating arteriole or ascending venule. Stalling capillary segments are marked with white arrows. Scale bars: 50  $\mu\text{m}$ . The example in (a) has a large number of stalling segments that is not representative of the other cases imaged. (d–e) Distributions of stalling and all (stalling PLUS nonstalling) capillary segments. A1–A5: Arterial-side capillaries with respective branching orders. A1 is the first capillary-size ( $<10 \mu\text{m}$  diameter) segment after the diving arteriole. V5–V1: Venous-side capillaries with respective branching orders. V1 is the last capillary-size segment before the ascending venule. Distributions are significantly different ( $\chi^2 = 27.05$ ,  $P < 0.001$ ), with a bias away from the first one to two branches downstream from arterioles and toward venules. (f) Comparison of stall durations in arterial and venous side segments. All stalls lasting longer than 1 min were found only on the venous side of the capillary network.

couple of arteriole branches downstream toward the venules (Figure 5(d) and (e)), it was striking that none of the arterial side stalls extended beyond 1 min. Although the majority of stalls were still short-lasting (less than 1 min) on the venous side, stalls longer than 1 min occurred exclusively on the distal end of the microcirculation (Figure 5(f)).

### RBC and plasma velocities in stalling segments

In another group of experiments ( $n = 2$ ) with acute cranial windows, we acquired OCT-angiogram time-series and dynamic light scattering (DLS)-OCT<sup>27,28</sup> sequentially within the same ROI (see supplementary methods). DLS-OCT enables us to robustly measure the velocities of the RBCs in capillaries and thus we are able to compare RBC velocities in stalling and nonstalling segments. After an 18-min OCT-angiogram acquisition, DLS-OCT data were acquired to get RBC velocities in capillary segments. Then, we administered 0.2 ml Intralipid<sup>®</sup> (i.a. in 1 min) to fill the plasma with

scattering particles (smaller than RBCs),<sup>29</sup> allowing measurement of plasma velocity in the same segments (Figure 6). We identified the stalling segments in this region from the angiogram time-series, determined the average RBC/plasma velocity within the segments and selected the same number of nonstalling segments randomly with the observer blinded to the capillary velocities. In stalling segments, both RBC and plasma velocities were significantly lower than their nonstalling counterparts (Figure 6(a) and (b)). Paired RBC and plasma velocity measurements revealed a fraction of stalling segments (9.4%) with comparably high plasma velocity (equal/higher than the mean plasma velocity of nonstalling segments), suggesting relatively slower RBCs than plasma in those segments during flowing conditions (Figure 6(c)).

### Sensitivity of OCT-angiography for capillary flow

It is important to understand the lower limit of RBC flow sensitivity in capillaries in order to determine if our

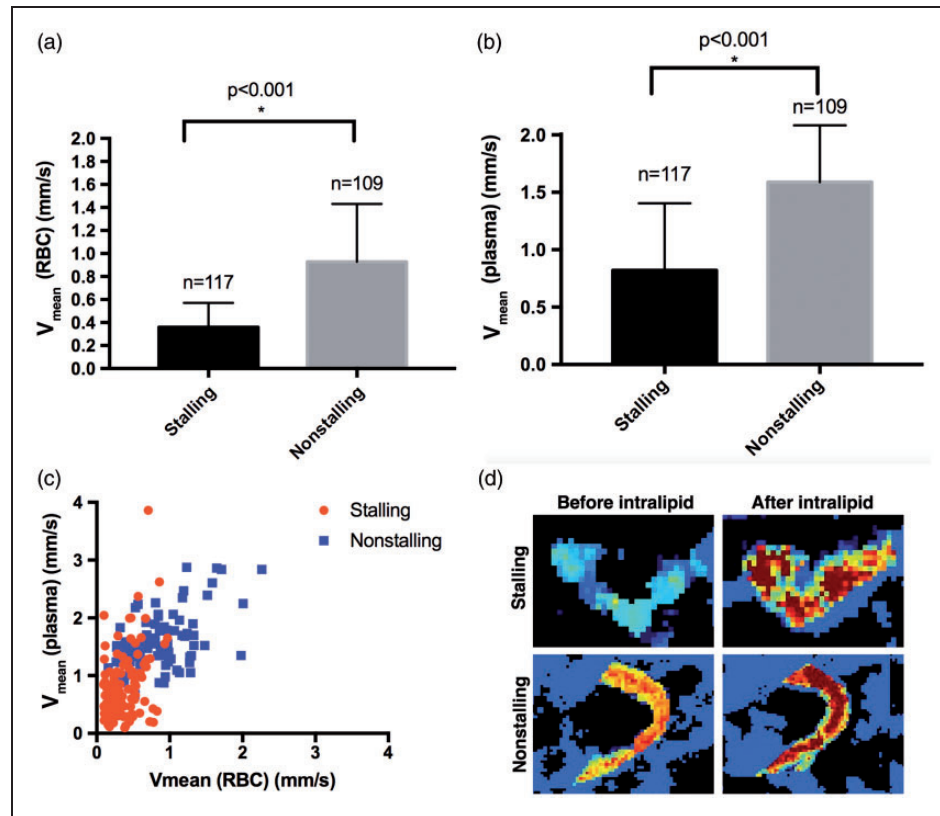


**Figure 6.** Differential RBC and plasma velocities in stalling vs. nonstalling capillaries. (a–b) Average RBC and plasma velocities in stalling vessels, even during flowing conditions are significantly lower than nonstalling vessels, as measured by DLS-OCT capillary velocimetry. (c) Scatter plot of average RBC and plasma velocities for each stalling and nonstalling segment. Both RBC and plasma velocities are lower in stalling segments. About 9.4% of stalling segments have plasma velocities equal to or higher than nonstalling segments. (d) Representative DLS-OCT images of capillary velocities in stalling and nonstalling segments, before and after intralipid injections.

observed stalls indicate an absolute cessation of RBC motion or if a relatively small amount of RBC motion was still possible. We performed a phantom experiment in which a static scattering surface was moving at varying constant horizontal velocities and the corresponding angiogram signal intensity was then calculated. We included the range 0.1–0.5 mm/s as this was the lower end of the physiological capillary velocity.<sup>30</sup> We also included values below 0.1 mm/s to account for sub-physiological velocities. We plotted the angiogram signal intensity difference between the motion and baseline conditions. The intensity difference was the highest above 0.3 mm/s, then it diminished between 0.2 and 0.02 mm/s, virtually disappearing at 0.01 mm/s, which is presumably the angiogram sensitivity for a horizontal velocity vector (supplementary figure). For an in vivo observation on sensitivity, we acquired angiograms in mice with five repeated B-scans for each B-line, instead of the regular two, which allowed us to compare angiogram signals acquired with varying B-scan intervals. Longer B-scan intervals provide higher sensitivity for particle motion.<sup>31–33</sup> For a total number of 100

consecutive stall events in four experiments, we were still able to identify 88 of those stalls in both two and five B-scan intervals. Twelve stalls were apparent in 2-B scan interval (8 ms) but were not detected in the 5-B scan interval (32 ms), suggesting a very slow RBC motion in these relatively few segments.

## Discussion

The cerebral microcirculation is a highly dynamic network specialized for efficient delivery of oxygen and nutrients to the brain. Our work expands our understanding of the hemodynamic principles governing capillary function under physiological conditions, utilizing the capabilities of OCT. We show that in awake mice and during rest, a significant portion of capillaries experience momentary cessation of moving blood cells. These interruptions in flow are brief, lasting from a few seconds to a minute, rarely up to a few minutes. Even though each individual stall is short-lasting, cumulatively, any given capillary segment that experienced a stall, had a cessation of flow for ~5% of the 9-min

observation time in awake, healthy mice. Functional hyperemia in awake animals had a profound effect on stalls, and during somatosensory activation significantly fewer stalls were observed than just before the stimulation. Although stalls were also relatively lower during stimulation than the post-stimulation period as well, this difference was not significant, implying that the return of stall parameters to baseline takes a longer time.

Stalls were repeatedly occurring in the same capillaries over a month, rather than randomly. In addition, stalling capillary segments were shown to have a slower RBC/plasma speed (measured between stalls) compared to nonstalling segments. The distribution of stalling capillaries followed the distribution of all segments, with a bias one to two branches away from the upstream end of the capillary network. Stalls lasting longer than 60 s were virtually always in downstream branches. The predisposition of stalls to the downstream side can be partly explained by the decreasing flow velocity ( $1.2 \pm 0.8$  mm/s in A1;  $0.7 \pm 0.3$  mm/s in V1) and pressure gradient arising from the larger cross-sectional area of capillaries on the venous versus the arteriole side of the capillary network in mice,<sup>34–38</sup> limiting the driving force for the cells passing through the segments and increasing the propensity for RBCs and leukocytes to stick to the wall.<sup>39</sup>

Anesthesia and acute cranial surgery exacerbated the stalls; a higher fraction of capillaries stalling with a longer duration in acute preparations and an increased number of segments involved under isoflurane. It should be considered that we had no blood pressure recording in the animals with chronic windows and the effect of isoflurane may be due to an expected 10–15 mmHg drop in mean blood pressure after induction<sup>40</sup> as this could reduce capillary RBC speed.

Capillaries with a cessation of RBC flow would be challenging to observe with only 0.5% to 3.5% of segments experiencing a stall at any given instant in awake and acute/anesthetized mice, respectively. The OCT-angiogram time-series allow imaging of  $\sim 200$  capillary segments in  $\sim 10$  s, and any given capillary segment signal vanishes when the motion of RBCs through the capillary stops, making the identification easy. Imaging of awake animals made it possible to indicate that these events were not merely a complication of anesthesia or surgery, but also physiological, and even responded to cortical activation. Combining OCT-angiograms with high signal-to-noise ratio fluorescent, TPM angiograms make it possible to overlap dynamic stall information with anatomical features, like capillary orientation and location within the microcirculatory network.

Previously, a TPM study showed that  $3 \pm 1\%$  of capillaries in anesthetized mice were stalled, based on time-lapse imaging of the motion of blood cells.<sup>17</sup>

The percentage of stalled capillaries increased 5- to 8-fold in mice with excessively high blood cell counts.<sup>17</sup> The increased number of blood cells, by increasing viscosity and clogging at capillary segments, can readily increase stalls. It is also likely that RBCs in some of these mouse models express adhesion proteins and stick to the capillary wall.<sup>41</sup> In diseased mice, stalls were persistent with median stall durations extending from 30 to 130 min, with very few stalled capillaries observed to reestablish flow during observation. In healthy mice, our observed stall durations were shorter, mostly lower than 30 s, with a small fraction extending up to more than 2 min. Even in mice with acute windows, we very rarely observed stalls lasting longer than 5 min. But in practically all cases, we saw a reestablishment of blood flow within the 9-min recording. Therefore, at least in our experiments with wild-type mice, we can conclude that stalls were short lasting and almost always temporary.

The OCT method is superior to TPM for identifying the temporal kinetics of stall events, since it allows uninterrupted monitoring of flow in hundreds of capillaries in few seconds. A TPM approach needs to focus on a limited number of segments with high magnification and a narrow field of view with the result that it is not practical to measure a large number of capillaries with a sufficiently long duration to characterize these temporal dynamics. Imaging of an equivalent number of capillaries to OCT-angiograms ( $\sim 200$  segments) would have a time resolution of minutes. The ability to image these stall events in a large field of view permits determination of the time-dependent distribution of stall events within a vascular network, which will provide sufficient data to guide simulations for assessing the hemodynamic effect of stalls on a microcirculatory network. It is possible that stalls persisting for 30–130 min, as observed by the previous TPM study in diseased mice,<sup>17</sup> are also present in our wild-type mice but that our OCT method is not revealing them as we need an image frame in which the capillary segment is not stalled in order for it to be revealed in the OCT-angiograms. A future study will have to carefully co-register TPM and OCT-angiogram data acquired in rapid succession in order to assess this. This combined imaging can enable identification of segments stalled for a longer duration than OCT time-series.

We had to use C57BL/6 strain mice in our chronic surgeries due to their decreased predisposition to neuro-inflammation.<sup>42</sup> Only females were included because of their calm behavior, easier housing and to prevent sex-dependent-variability since estrogen and testosterone affect the vascular histology and binding of blood cells to endothelium.<sup>43,44</sup> In those animals, the dura was kept intact to preserve cerebral physiology for the extended chronic imaging. The difference of strains

and surgical preparations between acute and chronic window groups would possibly affect the differences in stall characteristics. To account for any major differences, we did preliminary tests on C57BL/6 mice ( $n = 3$ ) with acute windows and intact dura. Average stall incidence ( $19.4 \pm 5.7\%$ ) and prevalence ( $3.5 \pm 2.1\%$ ) were comparable to our reported results on CD1. Performing an extensive comparison among different animal strains was beyond the scope of this work. However, detailed future work with relatively higher number animals to increase statistical power would elucidate differences between mouse strains, if any.

Inflammation underneath the cranial window would readily affect capillary flow properties with increased binding of blood cells to the endothelium. At least some degree of inflammation is inevitable during craniotomies. However, previous work suggested that even though subacute inflammatory changes would persist for up to two weeks after cranial window surgery, they would have mostly cleared by the end of the first month,<sup>45–47</sup> which was the minimum interval between our surgeries and imaging. We also administered corticosteroids and anti-inflammatory medications in the perioperative periods. Moreover, we did not see a change in the ratio of stalling segments between repeated imaging sessions over a one-month interval. If there were ongoing subacute inflammatory changes affecting the stalls in the first imaging session, they would at least decrease after one month and we would find a different ratio of stalls in the later sessions. Therefore, we believe that we can practically ignore the inflammation effect in our animals with chronic windows. Previous observations of similar capillary stalls in retina<sup>19</sup> also suggest that these stalling events may occur regardless of surgery.

A limitation in our methodology is that the detection of stalls depends on the imaging duration. Even though a 9-min recording identifies most of the stalls, we tend to detect at least 30% more stalling segments when we extend the observation to 18 min. Therefore, we can assume that with a limited amount of observation, we are always detecting a fraction of stalling capillaries, and this explains why we only observed a 50% overlap in stalling capillaries when our recording was repeated one-week or week-month later. In theory, although not practical, if we could record and analyze even longer durations, we would possibly identify all stalling segments. The current need for manually counting the stalling segments is a limitation for extended recordings but automated algorithms, if developed, can improve this analysis. Another criticism would be that our analysis is limited to the same cortical depth, around 150–250  $\mu\text{m}$  below the brain surface. OCT signal quality drops with increasing depth and detecting stalls require unaveraged single time-point angiogram data which can

have low signal-to-noise ratio. Parameters of stall kinetics could be differing across different cortical layers.

Our OCT-angiogram signals in capillaries are generated by the motion of blood cells, mostly RBCs. With a drop-out in angiogram signal, we are assuming that RBC flow has ceased, which may not always be the case. We performed a phantom experiment to measure the sensitivity of our imaging and found that we could detect an angiogram signal with a minimum 0.02 mm/s velocity. Other work on angiogram sensitivity also indicated that OCT-angiography is sensitive enough to image very slow blood flow at  $\sim 0.004$  mm/s.<sup>31,32,48</sup> Since average RBC velocity in capillaries is within the range 0.2–1.6 mm/s,<sup>30</sup> we are assuming that we are detecting capillaries with practically no RBC flow as stalling vessels. However, this may not always be the case for two reasons: Firstly, since we are manually identifying the stalling segments, the human eye may not be able to differentiate the low angiogram signals generated by transverse velocities slower than 0.05 mm/s from the background, being easily biased to mark these as no-flow. Secondly, our phantom experiments did not test for axial velocity sensitivity, which may be different from transverse velocity and also the sensitivity for actual RBC flow may be different from motion of a phantom scattering surface. Another limitation was that OCT could not determine whether stalling segments had RBCs stuck in them or had no RBCs at all, serving as “plasma channels”.<sup>49,50</sup> In fact, it is possible that the fraction of stalling segments with very high plasma velocity compared to RBC velocity would belong to such a group, the physiological significance remains to be determined. Finally, we did not systematically compare different cortical areas, being limited by the size of the cranial window. The stall parameters may be varying across different cortical regions, which would be another point for future investigation.

Diseases of small vessels are common causes of progressive disability and cognitive decline, especially in the elderly, with contribution from cardiovascular risk factors like hypertension and diabetes.<sup>4,51,52</sup> Changes in capillary morphology play an important role in microcirculatory dysfunction.<sup>51,53</sup> However, evaluation of dynamic flow patterns is also crucial,<sup>54–56</sup> but it is more difficult, since this requires imaging techniques with high spatiotemporal resolution. To enhance oxygen delivery, capillary flow patterns should homogenize when metabolism increases as heterogeneous velocities across a network diminishes the oxygen extraction.<sup>54,57–59</sup> Capillary dysfunction ends up with a diminished functional hemodynamic response and oxygen extraction.<sup>52</sup> Our observation of the lower prevalence of capillary stalls during functional activation may contribute to optimization of

microcirculatory flow patterns. Excessive capillary stalls, on the other hand, can be another feature of capillary dysfunction impairing cerebral perfusion or limiting oxygen extraction by increasing flow heterogeneity.<sup>52,54</sup> The effect of individual stalls on cerebral oxygenation, which was beyond the methodological capabilities of this study, is an intriguing point to address. Under physiological conditions, it can be expected that oxygen would be largely extracted in the first few branches after the precapillary arteriole<sup>25</sup> and it remains to be investigated if stalls on the downstream end of the microcirculation have a profound impact on tissue oxygenation. The relatively lower prevalence of capillary stalls during functional hyperemia can be a passive adaptation to the increased flow velocity so that more oxygen would be available for the downstream branches to extract. Whether this functional stall modulation actually represents a reserve for increased demand, however, can be questioned, especially considering that most capillaries (>99%) were already flowing under resting conditions, in line with previous work.<sup>20</sup> On the other hand, these baseline and activated capillary stalls may be different in pathologies and could be causing dynamic oxygenation problems within the cortex. All these interesting points remain to be determined by future work utilizing advanced techniques for dynamic monitoring of tissue oxygen with high spatiotemporal resolution.<sup>60</sup>

With this work, we conclude that RBC stalls in cerebral capillaries under physiological conditions in mice are frequent and consistent events. These stalls, which may not be detected by static imaging, can be quantified by OCT-angiography time-series efficiently. Acute cranial surgery and anesthesia result in a higher number of stalls compared to awake animals with chronic windows. Future investigation of these dynamics would reveal their impact on tissue perfusion and oxygenation even with normal pial arterial flow and a relatively normal capillary morphology. Investigation of the frequency, distribution and duration of capillary stalls can be exploited to better understand the diseases with capillary dysfunction and our method can be easily applied to different experimental models.

## Funding

The author(s) disclosed receipt of the following financial support for the research, authorship, and/or publication of this article: This study was supported by NIH grants R01-EB021018, P41-EB015896 and P01-NS055104, and the Air Force Office of Sponsored Research (AFOSR FA-9550-15-1-0473). The authors also would like to acknowledge the Shared Instrumentation Grants (1S10RR023043) that support the cluster in the Martinos Center for Biomedical Imaging. Şefik Evren Erdener's work was additionally supported by the Turkish Neurological Society.

## Acknowledgements

We thank Buyin Fu for his extensive efforts in animal preparations.

## Declaration of conflicting interests

The author(s) declared no potential conflicts of interest with respect to the research, authorship, and/or publication of this article.

## Authors' contributions

ŞEE, CBS and DAB conceived the study and designed the experiments. ŞEE, JT and KK collected the data. Ş.E.E, J.T, A.S and S.K. analyzed and interpreted the data. ŞEE, KK and JT drafted and CBS, and DAB critically revised the article. All authors approved the final version.

## Supplementary material

Supplementary material for this paper can be found at the journal website: <http://journals.sagepub.com/home/jcb>

## References

- Schlageter KE, Molnar P, Lapin GD, et al. Microvessel organization and structure in experimental brain tumors: microvessel populations with distinctive structural and functional properties. *Microvasc Res* 1999; 58: 312–328.
- De Silva TM and Faraci FM. Microvascular dysfunction and cognitive impairment. *Cell Mol Neurobiol* 2016; 36: 241–258.
- Iadecola C. The pathobiology of vascular dementia. *Neuron* 2013; 80: 844–866.
- Pantoni L. Cerebral small vessel disease: from pathogenesis and clinical characteristics to therapeutic challenges. *Lancet Neurol* 2010; 9: 689–701.
- Hall CN, Reynell C, Gesslein B, et al. Capillary pericytes regulate cerebral blood flow in health and disease. *Nature* 2014; 508: 55–60.
- Harb R, Whiteus C, Freitas C, et al. In vivo imaging of cerebral microvascular plasticity from birth to death. *J Cereb Blood Flow Metab* 2013; 33: 146–156.
- Ren H, Du C and Pan Y. Cerebral blood flow imaged with ultrahigh-resolution optical coherence angiography and Doppler tomography. *Opt Lett* 2012; 37: 1388–1390.
- Sakadzic S, Roussakis E, Yaseen MA, et al. Cerebral blood oxygenation measurement based on oxygen-dependent quenching of phosphorescence. *J Vis Exp* 2011; 4: pii: 1694.
- Hu S, Maslov K, Tsytsarev V, et al. Functional transcranial brain imaging by optical-resolution photoacoustic microscopy. *J Biomed Opt* 2009; 14: 040503.
- Yata K, Nishimura Y, Unekawa M, et al. In vivo imaging of the mouse neurovascular unit under chronic cerebral hypoperfusion. *Stroke* 2014; 45: 3698–3703.
- Srinivasan VJ, Mandeville ET, Can A, et al. Multiparametric, longitudinal optical coherence tomography imaging reveals acute injury and chronic recovery in experimental ischemic stroke. *PLoS One* 2013; 8: e71478.

12. Sword J, Masuda T, Croom D, et al. Evolution of neuronal and astroglial disruption in the peri-contusional cortex of mice revealed by in vivo two-photon imaging. *Brain* 2013; 136(Pt 5): 1446–1461.
13. Jia Y, Li P and Wang RK. Optical microangiography provides an ability to monitor responses of cerebral microcirculation to hypoxia and hyperoxia in mice. *J Biomed Opt* 2011; 16: 096019.
14. Jia Y, Grafe MR, Gruber A, et al. In vivo optical imaging of revascularization after brain trauma in mice. *Microvasc Res* 2011; 81: 73–80.
15. Takano T, Han X, Deane R, et al. Two-photon imaging of astrocytic Ca<sup>2+</sup> signaling and the microvasculature in experimental mice models of Alzheimer's disease. *Ann N Y Acad Sci* 2007; 1097: 40–50.
16. Ostergaard L, Engedal TS, Aamand R, et al. Capillary transit time heterogeneity and flow-metabolism coupling after traumatic brain injury. *J Cereb Blood Flow Metab* 2014; 34: 1585–1598.
17. Santisakultarm TP, Paduano CQ, Stokol T, et al. Stalled cerebral capillary blood flow in mouse models of essential thrombocythemia and polycythemia vera revealed by in vivo two-photon imaging. *J Thromb Haemost* 2014; 12: 2120–2130.
18. Mairey E, Genovesio A, Donnadiou E, et al. Cerebral microcirculation shear stress levels determine *Neisseria meningitidis* attachment sites along the blood-brain barrier. *J Exp Med* 2006; 203: 1939–1950.
19. Guevara-Torres A, Joseph A and Schallek JB. Label free measurement of retinal blood cell flux, velocity, hematocrit and capillary width in the living mouse eye. *Biomed Opt Exp* 2016; 7: 4228–4249.
20. Villringer A, Them A, Lindauer U, et al. Capillary perfusion of the rat brain cortex. An in vivo confocal microscopy study. *Circ Res* 1994; 75: 55–62.
21. Srinivasan VJ, Atochin DN, Radhakrishnan H, et al. Optical coherence tomography for the quantitative study of cerebrovascular physiology. *J Cereb Blood Flow Metab* 2011; 31: 1339–1345.
22. Srinivasan VJ, Jiang JY, Yaseen MA, et al. Rapid volumetric angiography of cortical microvasculature with optical coherence tomography. *Opt Lett* 2010; 35: 43–45.
23. Helmberger M, Pienn M, Urschler M, et al. Quantification of tortuosity and fractal dimension of the lung vessels in pulmonary hypertension patients. *PLoS One* 2014; 9: e87515.
24. Santisakultarm TP, Cornelius NR, Nishimura N, et al. In vivo two-photon excited fluorescence microscopy reveals cardiac- and respiration-dependent pulsatile blood flow in cortical blood vessels in mice. *Am J Physiol Heart Circ Physiol* 2012; 302: H1367–H1377.
25. Sakadzic S, Mandeville ET, Gagnon L, et al. Large arteriolar component of oxygen delivery implies a safe margin of oxygen supply to cerebral tissue. *Nat Commun* 2014; 5: 5734.
26. Blinder P, Tsai PS, Kaufhold JP, et al. The cortical angiome: an interconnected vascular network with non-columnar patterns of blood flow. *Nat Neurosci* 2013; 16: 889–897.
27. Lee J, Wu W, Jiang JY, et al. Dynamic light scattering optical coherence tomography. *Opt Exp* 2012; 20: 22262–22277.
28. Tang J, Erdener SE, Fu B, et al. Capillary red blood cell velocimetry by phase-resolved optical coherence tomography. *Opt Lett* 2017; 42: 3976–3979.
29. Pan Y, You J, Volkow ND, et al. Ultrasensitive detection of 3D cerebral microvascular network dynamics in vivo. *Neuroimage* 2014; 103: 492–501.
30. Ivanov KP, Kalinina MK and Levkovich Yu I. Blood flow velocity in capillaries of brain and muscles and its physiological significance. *Microvasc Res* 1981; 22: 143–155.
31. An L, Qin J and Wang RK. Ultrahigh sensitive optical microangiography for in vivo imaging of microcirculations within human skin tissue beds. *Opt Exp* 2010; 18: 8220–8228.
32. Wang RK, An L, Francis P, et al. Depth-resolved imaging of capillary networks in retina and choroid using ultrahigh sensitive optical microangiography. *Opt Lett* 2010; 35: 1467–1469.
33. Zhang A, Zhang Q, Chen CL, et al. Methods and algorithms for optical coherence tomography-based angiography: a review and comparison. *J Biomed Opt* 2015; 20: 100901.
34. Linninger AA, Gould IG, Marinnan T, et al. Cerebral microcirculation and oxygen tension in the human secondary cortex. *Ann Biomed Eng* 2013; 41: 2264–2284.
35. Zweifach BW and Lipowsky HH. Quantitative studies of microcirculatory structure and function. III. Microvascular hemodynamics of cat mesentery and rabbit omentum. *Circ Res* 1977; 41: 380–390.
36. Pries AR, Secomb TW, Gaehtgens P, et al. Blood flow in microvascular networks. Experiments and simulation. *Circ Res* 1990; 67: 826–834.
37. Gould IG, Tsai P, Kleinfeld D, et al. The capillary bed offers the largest hemodynamic resistance to the cortical blood supply. *J Cereb Blood Flow Metab* 2017; 37: 52–68.
38. Eriksson E and Myrhage R. Microvascular dimensions and blood flow in skeletal muscle. *Acta Physiol Scand* 1972; 86: 211–222.
39. Boryczko K, Dzwiniel W and Yuen DA. Dynamical clustering of red blood cells in capillary vessels. *J Mol Model* 2003; 9: 16–33.
40. Hoffman WE, Edelman G, Kochs E, et al. Cerebral autoregulation in awake versus isoflurane-anesthetized rats. *Anesth Analg* 1991; 73: 753–757.
41. Wautier MP, El Nemer W, Gane P, et al. Increased adhesion to endothelial cells of erythrocytes from patients with polycythemia vera is mediated by laminin alpha5 chain and Lu/BCAM. *Blood* 2007; 110: 894–901.
42. Nikodemova M and Watters JJ. Outbred ICR/CD1 mice display more severe neuroinflammation mediated by microglial TLR4/CD14 activation than inbred C57Bl/6 mice. *Neuroscience* 2011; 190: 67–74.
43. Cid MC, Kleinman HK, Grant DS, et al. Estradiol enhances leukocyte binding to tumor necrosis factor (TNF)-stimulated endothelial cells via an increase in TNF-induced adhesion molecules E-selectin, intercellular

- adhesion molecule type 1, and vascular cell adhesion molecule type 1. *J Clin Invest* 1994; 93: 17–25.
44. Kelly DM and Jones TH. Testosterone: a vascular hormone in health and disease. *J Endocrinol* 2013; 217: R47–R71.
  45. Dorand RD, Barkauskas DS, Evans TA, et al. Comparison of intravital thinned skull and cranial window approaches to study CNS immunobiology in the mouse cortex. *Intravital* 2014; 3: e29728.
  46. Holtmaat A, Bonhoeffer T, Chow DK, et al. Long-term, high-resolution imaging in the mouse neocortex through a chronic cranial window. *Nat Protoc* 2009; 4: 1128–1144.
  47. Nishiyama N, Colonna J, Shen E, et al. Long-term in vivo time-lapse imaging of synapse development and plasticity in the cerebellum. *J Neurophysiol* 2014; 111: 208–216.
  48. Wei W, Xu J, Baran U, et al. Intervolume analysis to achieve four-dimensional optical microangiography for observation of dynamic blood flow. *J Biomed Opt* 2016; 21: 36005.
  49. Hauck EF, Apostel S, Hoffmann JF, et al. Capillary flow and diameter changes during reperfusion after global cerebral ischemia studied by intravital video microscopy. *J Cereb Blood Flow Metab* 2004; 24: 383–391.
  50. Hudetz AG, Spaulding JG and Kiani MF. Computer simulation of cerebral microhemodynamics. *Adv Exp Med Biol* 1989; 248: 293–304.
  51. Wardlaw JM, Smith C and Dichgans M. Mechanisms of sporadic cerebral small vessel disease: insights from neuroimaging. *Lancet Neurol* 2013; 12: 483–497.
  52. Ostergaard L, Engedal TS, Moreton F, et al. Cerebral small vessel disease: capillary pathways to stroke and cognitive decline. *J Cereb Blood Flow Metab* 2016; 36: 302–325.
  53. Wardlaw JM, Doubal FN, Valdes-Hernandez M, et al. Blood-brain barrier permeability and long-term clinical and imaging outcomes in cerebral small vessel disease. *Stroke* 2013; 44: 525–527.
  54. Jespersen SN and Ostergaard L. The roles of cerebral blood flow, capillary transit time heterogeneity, and oxygen tension in brain oxygenation and metabolism. *J Cereb Blood Flow Metab* 2012; 32: 264–277.
  55. Ostergaard L, Jespersen SN, Mouridsen K, et al. The role of the cerebral capillaries in acute ischemic stroke: the extended penumbra model. *J Cereb Blood Flow Metab* 2013; 33: 635–648.
  56. Ostergaard L, Aamand R, Gutierrez-Jimenez E, et al. The capillary dysfunction hypothesis of Alzheimer's disease. *Neurobiol Aging* 2013; 34: 1018–1031.
  57. Stefanovic B, Hutchinson E, Yakovleva V, et al. Functional reactivity of cerebral capillaries. *J Cereb Blood Flow Metab* 2008; 28: 961–972.
  58. Schulte ML, Wood JD and Hudetz AG. Cortical electrical stimulation alters erythrocyte perfusion pattern in the cerebral capillary network of the rat. *Brain Res* 2003; 963: 81–92.
  59. Kleinfeld D, Mitra PP, Helmchen F, et al. Fluctuations and stimulus-induced changes in blood flow observed in individual capillaries in layers 2 through 4 of rat neocortex. *Proc Natl Acad Sci U S A* 1998; 95: 15741–15746.
  60. Xu K, Boas DA, Sakadzic S, et al. Brain tissue PO<sub>2</sub> measurement during normoxia and hypoxia using two-photon phosphorescence lifetime microscopy. *Adv Exp Med Biol* 2017; 977: 149–153.